ADVANCES IN ATMOSPHERIC SCIENCES, VOL. 34, JANUARY 2017, 79–87

• **Original Paper** •

Comparison between the Response of the Northwest Pacific Ocean and the South China Sea to Typhoon Megi (2010)

Zi-Liang LI*[1] and Ping WEN[1,2]

[1]*Physical Oceanography Laboratory, College of Oceanic and Atmospheric Sciences, Ocean University of China, Qingdao* 266100, *China*

[2]*Hunan Provincial Meteorological Station, Changsha* 430100, *China*

(Received 28 January 2016; revised 19 June 2016; accepted 21 July 2016)

ABSTRACT

The upper-ocean responses to Typhoon Megi (2010) are investigated using data from ARGO floats and the satellite TMI. The experiments are conducted using a three-dimensional Princeton Ocean Model (POM) to assess the storm, which affected the Northwest Pacific Ocean (NWP) and the South China Sea (SCS). Results show that the upwelling and entrainment experiment together account for 93% of the SST anomalies, where typhoon-induced upwelling may cause strong ocean cooling. In addition, the anomalous SST cooling is stronger in the SCS than in the NWP. The most striking feature of the ocean response is the presence of a two-layer inertial wave in the SCS—a feature that is absent in the NWP. The near-inertial oscillations can be generated as typhoon wakes, which have maximum flow velocity in the surface mixed layer and may last for a few days, after the typhoon's passage. Along the typhoon tracks, the horizontal currents in the upper ocean show a series of alternating negative and positive anomalies emanating from the typhoon.

Key words: typhoon, South China Sea, Northwest Pacific, upwelling, entrainment, near-inertial oscillation

Citation: Li, Z.-L., and P. Wen, 2016: Comparison between the response of the Northwest Pacific Ocean and the South China Sea to Typhoon Megi (2010). *Adv. Atmos. Sci.*, **34**(1), 79–87, doi: 10.1007/s00376-016-6027-9.

1. Introduction

Studying the upper-ocean response to typhoons began as early as the 1950s and 1960s (Fisher, 1958; Miller, 1964; Leiper, 1967; O'Brien, 1967; O'Brien and Reid, 1967). Typhoon cyclonic wind stress causes strong upper-ocean vertical mixing and cooling of the SST (Price, 1981; Greatbatch, 1985; Stramma et al., 1986; Gjevik, 1991; Gjevik and Merrifield, 1993; Sakaida et al., 1998; Morey et al., 2006; Yun et al., 2012; Choi et al., 2013; Mei and Pasquero, 2013), which can adversely affect typhoon intensity change and structural evolution (Chang and Anthes, 1979; Bender and Ginis, 2000; Elsner et al., 2013). Another consideration is that the pumping and entrainment as a result of the typhoon will make the ocean mixed-layer depth (MLD) deepen (Halpern, 1974; Elsberry et al., 1976).

The South China Sea (SCS) is an ocean basin often affected by typhoons, and thus has drawn considerable interest for more than a decade (Chu et al., 2000; Lin et al., 2003a, 2003b; Shang et al., 2008; Tseng et al., 2010; Chen et al., 2012). Typhoon-induced wind stress may play a significant role in SCS circulation and near-inertial oscillation (Chu et al., 2000; Ko et al., 2014). It may also cause many significant changes in ocean wave characteristics, such as significant wave heights and wave propagation, wherein the maximum wave heights appear in the front-right quadrant of the typhoon center (Wang et al., 2014). The upper-ocean response to a typhoon is an important component of ocean—air interaction. Numerous coupled atmosphere–ocean–wave models have been developed in order to understand the response of the ocean to tropical cyclones (Large and Crawford, 1995; Liu et al., 2013).

The ocean response when a typhoon passes over the NWP differs significantly to that of the SCS (Lin, 2012; Mei et al., 2015a). Since the mixed layer in the SCS is in general shallower than that in the NWP, the typhoon-generated SST cooling is expected to be stronger in the SCS than that in the NWP (Mei et al., 2015b). Numerous studies have been devoted to exploring the typhoon-generated SST cooling in the SCS (Chu et al., 2000; Lin et al., 2003a, 2003b; Tsai et al., 2012) and the NWP (Lin, 2012; Yang et al., 2012). Understanding the air–sea interaction associated with a typhoon is critical for improving typhoon intensity and track forecasting. Note also that there are few studies that have helped to advance our understanding of the possible mechanism involved in the generation of the internal wave when a typhoon passes over the SCS or the NWP (Shay and Elsberry, 1987;

* Corresponding author: Zi-Liang LI
Email: liziliang@ouc.edu.cn

Oey et al., 2008; Guan et al., 2014). The present study seeks to fill this knowledge gap, and we report our findings in this paper as follows. An introduction to Typhoon Megi (2010) is provided in section 2, followed by a description of POM in section 3. We compare the response of the SCS and NWP to Typhoon Megi (2010) in section 4, and then conclusions are given in section 5.

2. Typhoon Megi (2010)

Typhoon Megi (2010), which was the most intense typhoon in 2010 worldwide, formed as a tropical depression over southwestern Guam (11.8°N,140.9°E) on 13 October and intensified into a tropical storm that evening. On 15 October, Megi (2010) intensified into a typhoon over the Pacific to the east of the Philippines (Fig. 1). Megi became a super typhoon on 17 October, reaching a peak intensity of maximum sustained winds of about 72 m s^{-1} near its center, and a minimum central pressure of 895 hPa (Fig. 1).

Along the track of Megi (2010), the moving speed of the typhoon was only 1.4–2.8 m s^{-1} in the SCS. However, the translation speed of the typhoon was 5.5–6.9 m s^{-1} east of the Philippines. Typhoon Megi (2010) was more intense over the NWP than over the SCS. Super Typhoon Megi (2010) crossed Luzon Island during 18–19 October and weakened to a typhoon over the northeastern part of the SCS on 22 October. Typhoon Megi (2010) made landfall over the coast of Fujian on 23 October and weakened into a tropical storm and dissipated on the morning of 24 October over Fujian. The data are from China Meteorological Administration–Shanghai Typhoon Institute Best Track Dataset for Tropical Cyclones over the NWP.

3. Data and methodology

The three-dimensional primitive equation circulation model, POM, is used to study the upper–ocean response to Typhoon Megi (2010). The computations of the model take place on $0.5^\circ \times 0.5^\circ$ curvilinear orthogonal horizontal coordinates and a sigma layer in the vertical coordinate with 16 layers at $\sigma = 0, -0.003125, -0.006250, -0.0125, -0.025, -0.05, -0.100, -0.200, -0.300, -0.400, -0.500, -0.600, -0.700, -0.800, -0.900$ and -1.000. The study domain covers 20°S to 45°N in latitude and 100°E to 70°W in longitude. The terrain data are from ETOPO5 ($5' \times 5'$). The minimum (maximum) water depth is 10 m (4500 m). The external and internal model time steps are 6 s and 180 s, respectively.

Surface boundary conditions are forced by sea surface wind, air–sea interface heat flux and vapor flux. The western and eastern boundaries are sheltered by land, while the climatological monthly averaged temperature and salinity data are employed in the northern and southern boundaries. Thus, the boundary set may be closed.

The model is initialized by the climatological mean temperature and salinity with a $1^\circ \times 1^\circ$ horizontal resolution and 33 levels provided by WOA05 (World Ocean Atlas 2005) (Antonov et al., 2006; Locarnini et al., 2006). The forcing of the model during the spin-up period and subsequent simulations requires the wind stress from NCEP reanalysis data at 6-h intervals (Kalnay et al., 1996), and the monthly sensible heat net flux and latent heat net flux from COADS (Slutz et al., 1985; Da Silva et al., 1994).

4. Results and discussion

4.1. *SST*

POM reproduces the maximum SST cooling and its location well; the comparison of the modeled SST drop with the corresponding TRMM images (Fig. 2) shows good agreement. The excessive cooling in POM is most likely due to the background temperature and salinity structure in the upper ocean. The strong pre-storm currents and fine resolution of POM may also contribute to the enhanced mixing during the storm's passage, and thus stronger SST cooling tends to

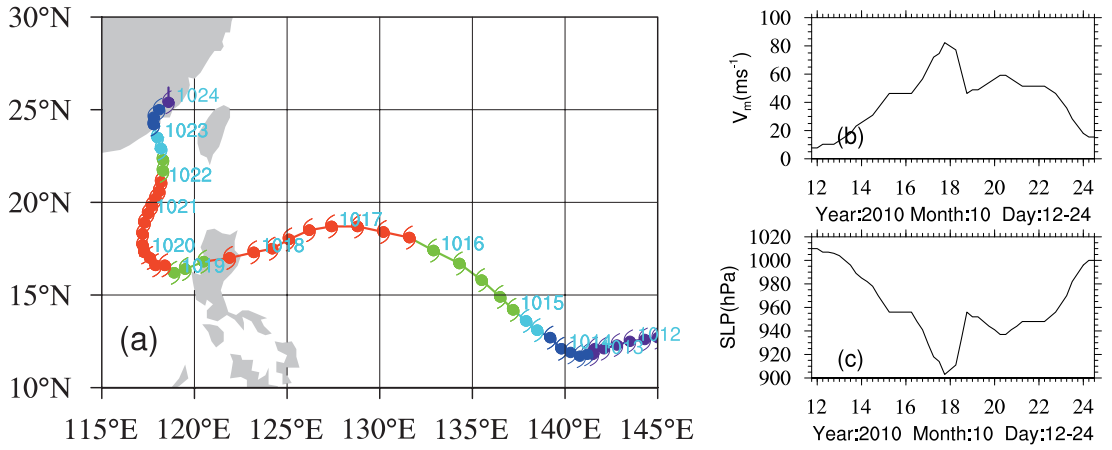

Fig. 1. The (a) track and (b, c) intensity change of the typhoon (minimum central pressure and maximum wind speed) from the JTWC best-track data.

be induced. Along the storm track, it is clear that the maximum sea surface cooling takes place in the SCS (10°–30°N, 110°–122°E). When the typhoon crosses the SCS, the maximum wind speed near the typhoon center reaches about 42–52 m s^{-1}. The stronger typhoon intensity, with slower moving speed of 1.4–2.8 m s^{-1}, plays a significant role in producing a stronger cooling in the SCS (Chiang et al., 2011; Ko et al., 2014). Figure 2 shows the diurnal average SST difference between 14 October and 24 October, which represents the maximum pre-storm minus post-storm SST in the SCS. It is evident that the maximum SST drop is more than 5.0°C after Typhoon Megi (2010) enters into the SCS. By comparison, Fig. 3 shows the diurnal average SST difference between 10 October and 17 October, which represents the maximum pre-storm minus post-storm SST in the NWP. The maximum sea surface cooling in the NWP (10°–30°N, 122°–145°E) is generally of a magnitude of 2.5°C, and the translation speed of Typhoon Megi (2010) reaches 7 m s^{-1} (25 km h^{-1}) and the maximum wind speed near the typhoon center reaches only about 32–42 m s^{-1}, when the typhoon crosses the NWP. Finally, note that the vertical temperature decreases from 29°C to 21°C at the depth of 13 m, and from 28.5°C to 21°C at the depth of 25 m, when the typhoon passed over the SCS. By comparison, the vertical temperature decreases from 28.5°C to 27°C at the depth of 13 m, and from 28°C to 27°C at the depth of 25 m, when the typhoon passes over the NWP.

4.2. *Strong upwelling and entrainment experiment*

4.2.1. *Experimental design*

The SST cooling is mainly due to vertical mixing and upwelling, in which the former of these two processes is associated with entrainment and the latter can be induced by Ekman pumping and near-inertial oscillations (Price, 1981; Shay and Elsberry, 1987; Price et al., 1994; Yablonsky and Ginis, 2009). Here, we present the results of two sensitivity experiments to evaluate the relative importance of upwelling and entrainment (Chiang et al., 2011).

EX1 (upwelling experiment): Attention is given to the important matter of choosing POM model parameters to best represent the upwelling process induced by Typhoon Megi

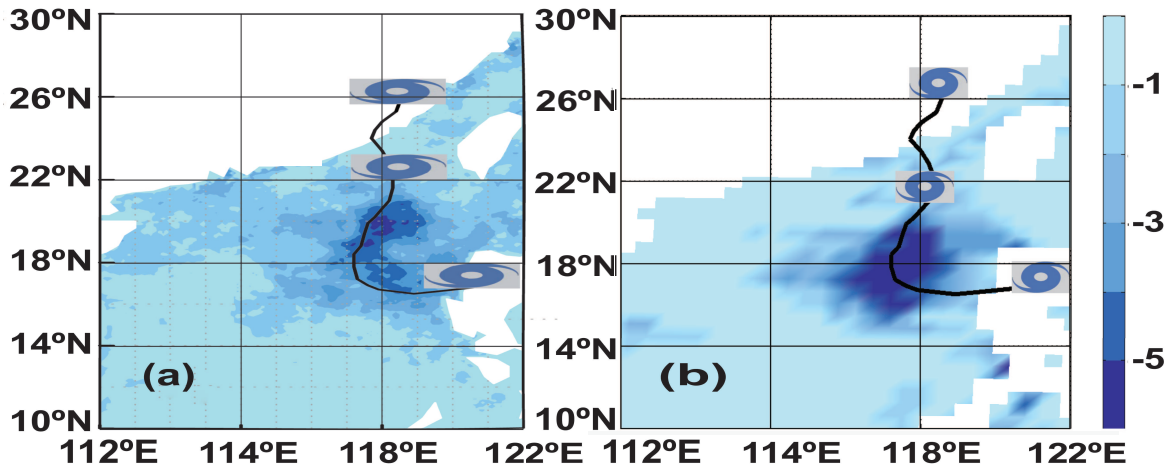

Fig. 2. The diurnal average SST difference (SCS) between 14 and 24 October from (a) TMI data and (b) POM.

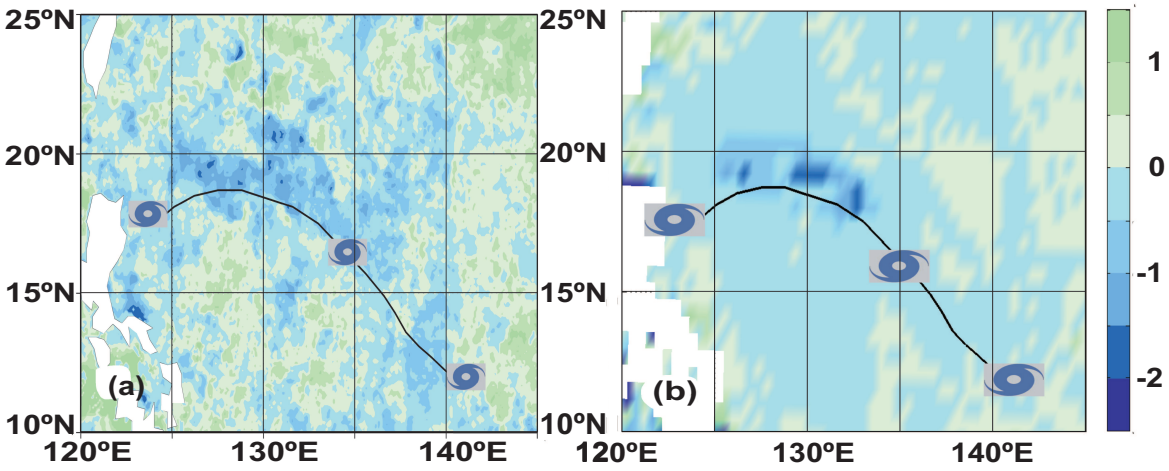

Fig. 3. The diurnal average SST difference (NWP) between 10 and 17 October from (a) TMI data and (b) POM.

(2010). We set the vertical kinematic viscosity coefficient (K_M) to 0.003 m^2 s^{-1} and the vertical diffusivity coefficient (K_H) to 0.004 m^2 s^{-1}. Because Ekman pumping is largely independent of K_M, and the chosen K_H value is about two orders of magnitude smaller than typical values found in the control experiment (CTL), during Typhoon Megi (2010), this experiment therefore simulates the upwelling component of the cooling process. The other model parameters and forcing remain unchanged (Chiang et al., 2011).

EX2 (entrainment experiment): Since the shear-induced mixing is a one-dimensional process, a one-dimensional ocean model may be sufficient for capturing the typhoon-induced SST anomalies. The one-dimensional experiments in this study are also performed using the same version of the three-dimensional ocean model (i.e., POM), except that the advection and pressure gradient terms are removed (Yablonsky and Ginis, 2009). The turbulence closure sub-model and the vertical advection and diffusion are identical to the three-dimensional model. Because one-dimensional models are limited by their inability to account for upwelling caused by Ekman pumping and other temperature fluctuations related to horizontal variations, the one-dimensional experiment is designed to simulate the vertical entrainment and mixing process (Chiang et al., 2011).

4.2.2. *Results of the experiments*

The most striking aspect of the experiment results is the difference in the typhoon-induced SST drop between the SCS and NWP. Figures 2b and 3b show the daily average SST difference induced by Typhoon Megi (2010) in the CTL experiment, where two maximum SST drops are taken as the sampling points to study the mechanism of the storm-induced SST drop. The first one is located in the SCS (18°N, 120°E), and the second in the NWP (19°N, 130°E).

The two sensitivity experiments are conducted to evaluate the relative importance of upwelling (EX1) and entrainment (EX2), respectively (Table 1). When typhoon Megi (2010) enters into the SCS, the maximum ΔSST decline in EX1 is about 3.9°C, and the maximum ΔSST drop in EX2 is about 1.5°C, as compared to the maximum ΔSST decline of 5.8°C in CTL. Therefore, 67% and 26% of the SST drop caused by Storm Megi (2010) is caused by upwelling and entrainment, respectively. By comparison, when Typhoon Megi (2010) passes over the NWP, the maximum ΔSST decline in EX1 is about 1.6°C, and the maximum ΔSST drop in EX2 is about 0.8°C, as compared to the maximum ΔSST decline of 2.6°C in CTL. Thus, 62% and 31% of the SST drop is induced by upwelling and entrainment, respectively. The ΔSSTs together account for 93% in both of these experiments, which agrees with the ΔSST in CTL and demonstrates that our designs for EX1 and EX2, to separate the upwelling and entrainment processes, are appropriate.

Table 1. List of experiments.

Experiment	Purpose	ΔSST Maximum		ΔSST (%)	
		SCS	NWP	SCS	NWP
CTL	Control	−5.8°C	−2.6°C	–	–
EX1	Upwelling	−3.9°C	−1.6°C	67	62
EX2	Entrainment	−1.5°C	−0.8°C	26	31

It is evident from Fig. 4 that strong upwelling, together with entrainment mixing, may significantly reduce the SST. From the time series, the SST begins to drop on a couple of consecutive days and reaches its minimum after the storm has passed. However, the SST drop through the mixing process is restored to its stabilized temperature after two consecutive days. It is noticeable that the typhoon-induced SST cooling in the SCS can be nearly twofold stronger than that in the NWP.

4.3. *MLD*

The vertical temperature profiles from a pair of ARGO floats before and after the typhoon are shown in Fig. 5, and agree well with that simulated by POM. The first ARGO float (R2901123) is located at (18.7°N, 118.7°E) in the SCS and the second (R5901571) at (14.8°N, 135°E) in the NWP, approximately 100 km away from the typhoon center. The

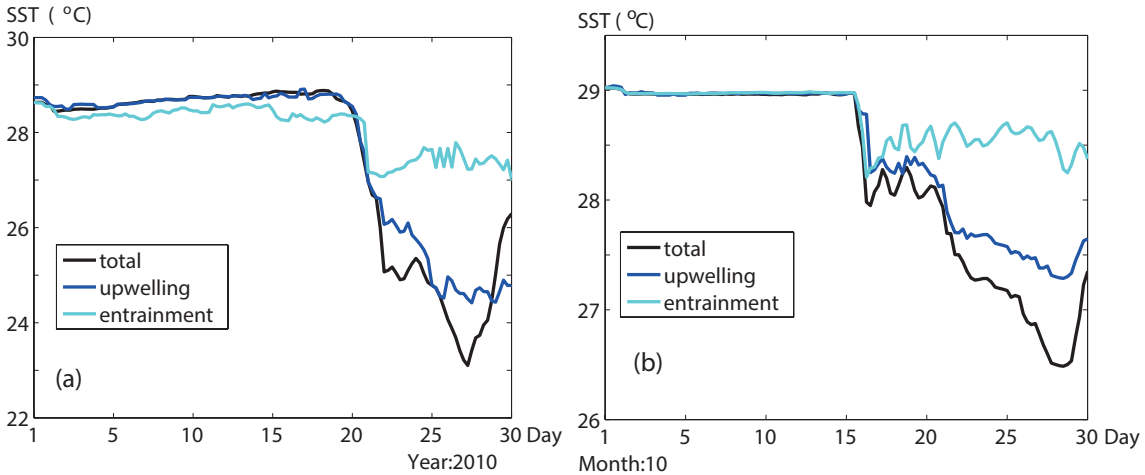

Fig. 4. A comparison of the time series of the SST drop between three sets of experiments in the (a) SCS (b) NWP.

oceanic mixed layer is typically defined as a layer of uniform temperature and density. Figure 5a shows that the MLD increases from 40 m to 60 m, and the mixed-layer temperature (MLT) decreases from 29.5°C to 28°C, when the typhoon enters into the SCS. By comparison, Fig. 5b shows that the pre-typhoon MLD is about 50 m, and the typhoon results in a deepening of the mixed layer up to 75 m; however, the MLT decreases from 29.8°C to 29.6°C, when the typhoon passes over the NWP.

Since the initial mixed layer is shallower in the SCS than in the NWP, typhoon-induced SST and MLT cooling is also expected to be stronger in the former region. The storm translation speed and its intensity can also affect the vertical entrainment and mixing of cold water from the lower layer into the surface layer (Chiang et al., 2011; Ko et al., 2014).

We determine the MLD using a density change of 0.125 in sigma-*t* from the ocean surface (Levitus, 1982). Figure 6 shows that the sigma-*t* deepening trends coincide with SST cooling on the right-hand side of the typhoon track in the SCS and NWP. Taking samples from the eastern side of the storm, a time series comparison between the diurnal average MLD is shown in Fig. 7. The MLD in the SCS shows an abrupt deepening trend from around 60 m in the pre-storm period to a depth of 120 m in post-storm period, and then restores steadily to 80 m on 31 October. In the NWP, however, the MLD shows weak temporal variation and ranges from 60 m to 80 m before and after the typhoon.

4.4. *Stratification and near-inertial oscillation*

The upper ocean response to a typhoon can be divided into two stages, the first of which is the forced stage, when the typhoon winds drive the mixed layer currents and cause the SST cooling, and the second of which is the relaxation stage, when the typhoon can excite inertial gravity oscillations with a near-inertial period (Gill, 1984; Garrett, 2001). Comparing Fig. 8 with Fig. 9, one can see that the response of the currents appears in the typhoon wake and that Typhoon Megi (2010) accelerates the near-inertial oscillations in the mixed layer. However, there are some remarkable features in that the ocean response to Typhoon Megi (2010) can create and

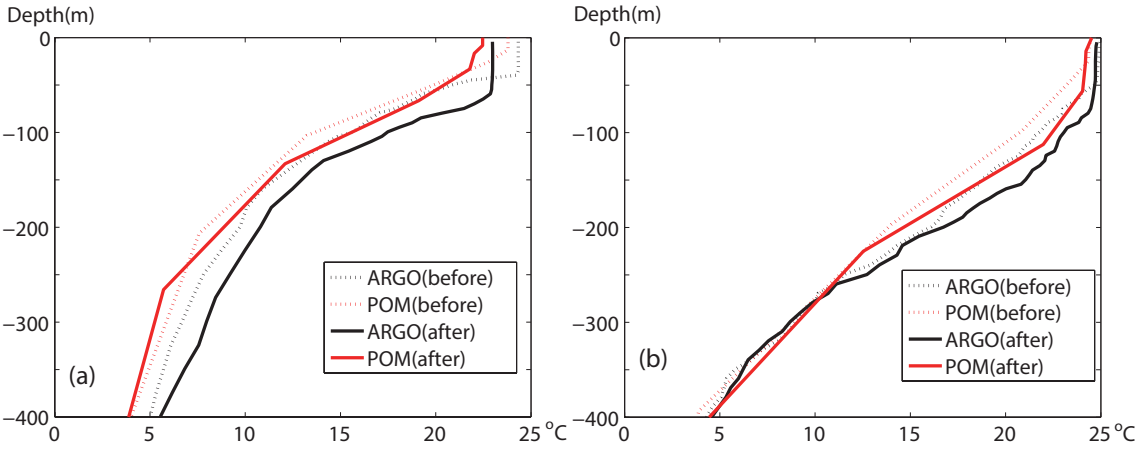

Fig. 5. Vertical temperature profiles from ARGO data and POM in the (a) SCS and (b) NWP.

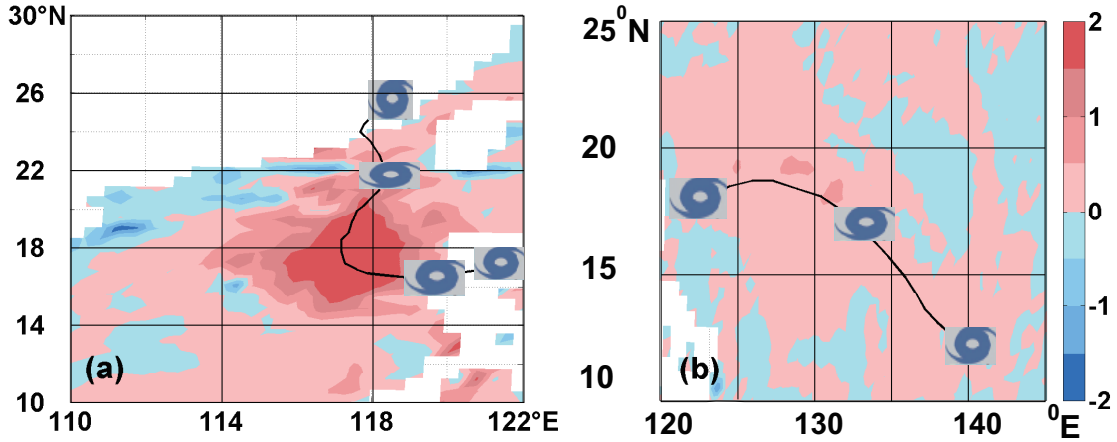

Fig. 6. The simulated (POM) diurnal average sigma-*t* (units: kg m^{-3}) difference between 14 and 24 October in the (a) SCS and (b) NWP.

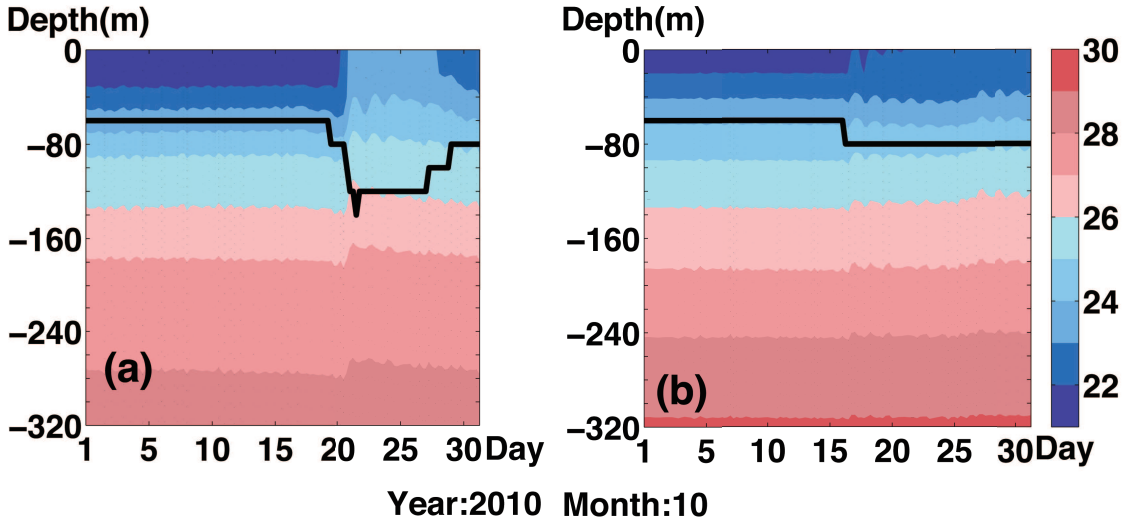

Fig. 7. The time–depth contours of sigma-*t* (black line for MLD; units: kg m^{-3}) before and after Megi (2010) entered the (a) SCS and (b) NWP.

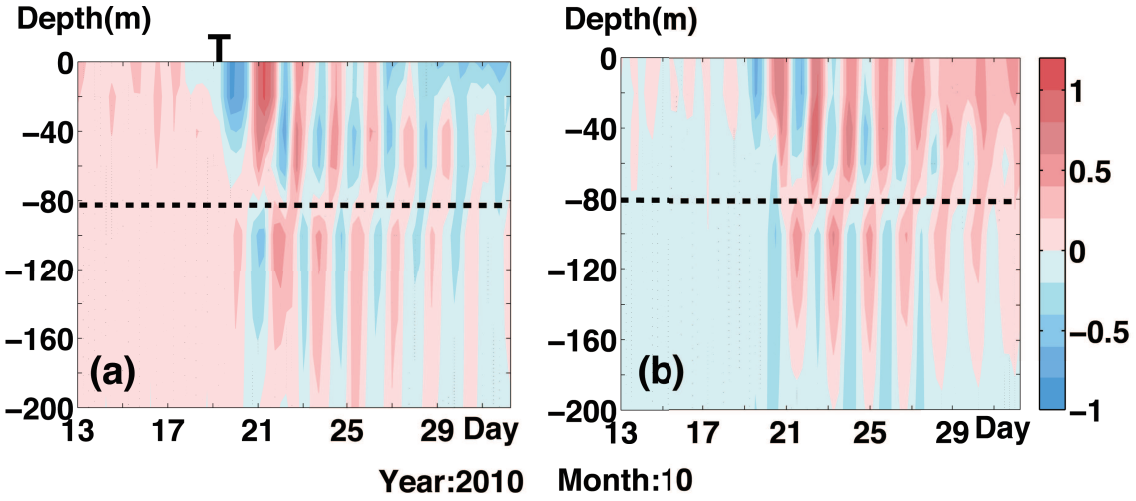

Fig. 8. The time–depth contours of the (a) east and (b) north near-inertial current components (units: m s^{-1}) at (16.5°N, 118°E) in the SCS ("T" for typhoon).

maintain a vertical layering near-inertial oscillation, layered at the depth of 80 m, when Typhoon Megi (2010) passes over the SCS (16.5°N, 118°E). The oscillations at the two levels are nearly out of phase, because there is distinct vertical thermal stratification in the SCS (Fig. 5). The opposing phase found in the SCS can be explained using a simple two-layer model (Millot and Crépon, 1981), which tends to disappear if the vertical thermal stratification weakens.

After the typhoon enters into the SCS on 20 October, the velocity of the current is fastest near the surface, with a maximum speed of about 1 m s^{-1}. The current slows to a second maximum speed of about 0.5 m s^{-1} at the depth of 120 m. However, a relatively weak and quickly damped near-inertial flow occurs in the NWP (17.5°N, 131°E), with a maximum near-inertial speed of approximately 0.8 m s^{-1} in the upper mixed layer, after Typhoon Megi (2010) passes over the NWP on 17 October. The important point here is that the simulated diurnal current vectors rotate clockwise at the depth of 30 m, when Typhoon Megi (2010) passes over the SCS (16.5°N, 118°E) and the NWP (17.5°N, 131°E). Before Typhoon Megi (2010), the simulated diurnal currents are extremely weak (only 0.1–0.2 m s^{-1}). During the passage of Megi (2010), the diurnal currents gradually increase to a maximum speed of about 1 m s^{-1}, which lasts for about 8 days in the SCS and 12 days in the NWP.

In order to further reveal the diurnal variations of the currents, the power density spectra of the eastward and northward components of current velocities are calculated and shown in Fig. 10. One can see that the period of the near-inertial oscillation is 1.7 days, which is smaller than the local inertial period of 1.78 days at (16.5°N, 118°E) in the SCS. The frequencies are 4.6% higher than the local inertial frequency, which is the so-called blue shift. By comparison, the near-inertial oscillation period is 1.62 days, which is smaller

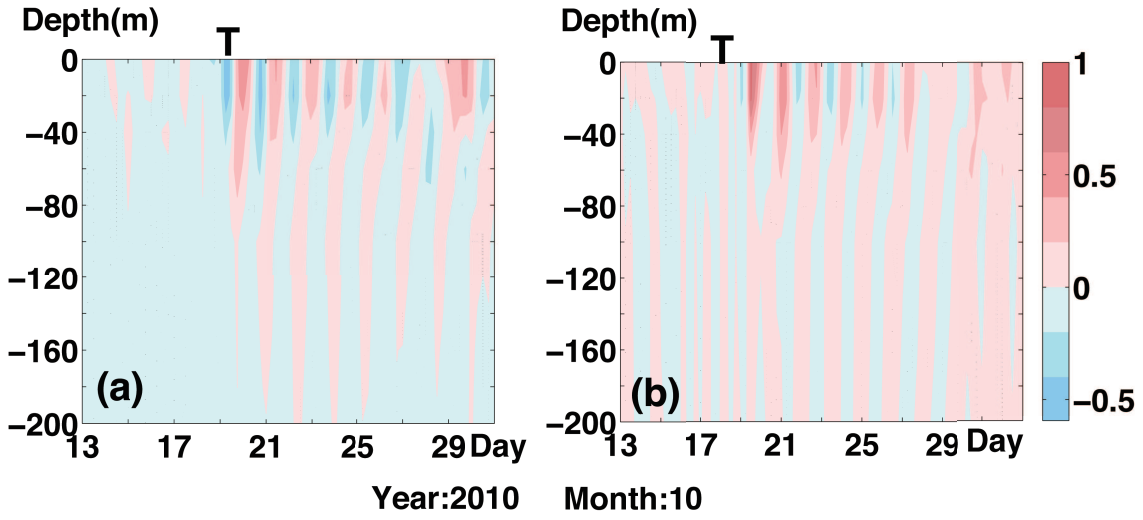

Fig. 9. The time–depth contours of the (a) east and (b) north near-inertial current components (units: m s^{-1}) at (17.5°N, 131°E) in the NWP ("T" for typhoon).

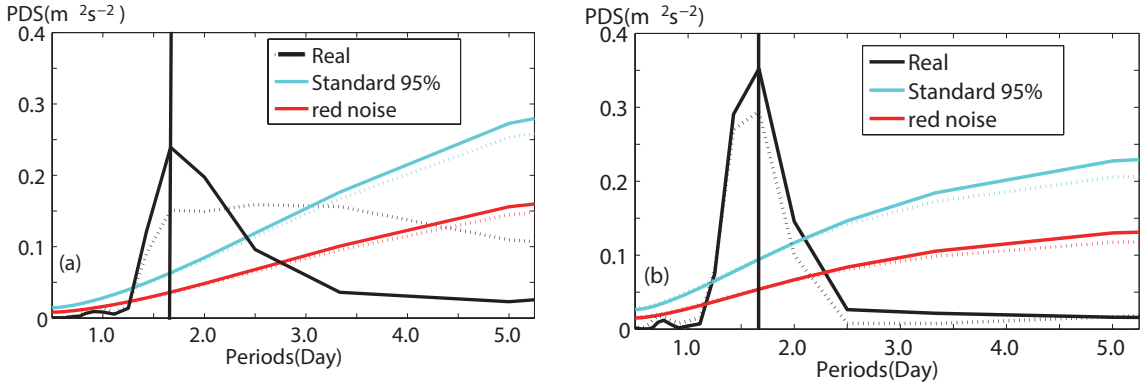

Fig. 10. Power density spectra (units: m^2 s^{-2}) of the east and north current components (a) at (16.5°N, 118°E) in the SCS and (b) at (17.5°N, 131°E) in the NWP.

than the local inertial period of 1.66 days at (17.5°N, 131°E) in the NWP. The frequencies are 2.5% higher than the local inertial frequency.

4.5. *Vertical velocity*

Waves with alternating upwelling and downwelling cells are left behind Typhoon Megi (2010) both in the SCS and NWP. The moving speed of Typhoon Megi (2010) does not exceed 2.8 m s^{-1} in the SCS, while it reaches 7 m s^{-1} in the NWP. Geisler (1970) indicated that, for a fast-moving storm, the upward motion is located beneath the rear of the storm center. For a slow-moving storm, however, the upward motion is mainly located around the storm center. It should be noted that upwelling (with a maximum 1.5 mm s^{-1}) is evident when Typhoon Megi (2010) passes over the SCS, which is consistent with earlier work on the impacts on the upper ocean of moving typhoons (Shay et al., 1992; Zedler et al., 2002). However, in the NWP, along the Typhoon Megi (2010) track, the upwelling with maximum amplitude (0.9 mm s^{-1}) is located in the region of a quarter wavelength behind the typhoon center.

Studies are currently underway to estimate the relationship between SST and vertical velocities, which shows a sharp transition at the depth of 48 m. The vertical velocity increases from 2.5×10^{-4} m s^{-1} to 7.5×10^{-4} m s^{-1}, and SST decreases from 28.75°C to 22.5°C, when the typhoon enters into the SCS. By comparison, the vertical velocity at 48 m increases from 2.0×10^{-4} m s^{-1} to 5.0×10^{-4} m s^{-1}, and SST decreases from 29°C to 27.7°C, when the typhoon passes over the NWP. Comparisons at other depths yield similar results; the primary difference is that the vertical velocities decay too rapidly with depth.

The last comparison involves the vertical velocities and sigma-*t* at the depth of 25 m. The vertical velocity at 25 m increases from 2.0×10^{-4} m s^{-1} to 4.0×10^{-4} m s^{-1}, and the sigma-*t* increases from 21.5 kg m^{-3} to 25 kg m^{-3}, when the typhoon enters into the SCS. By comparison, the vertical velocity at 25 m increases from 1.0×10^{-4} m s^{-1} to 3.0×10^{-4} m s^{-1}, and the sigma-*t* increases from 22 kg m^{-3} to 22.5 kg m^{-3}, when the typhoon passes over the NWP.

5. Conclusion

Typhoons moving over an ocean represent an extreme case of air–sea interaction. They are known to generate a vigorous response in the underlying ocean, which can include strong upper-ocean currents, the generation and propagation of near-inertial oscillation, and the formation of a cold wake beneath the storm. Typhoons over the SCS and NWP exhibit significant differences in storm track, translation speed and intensity, which are affected by the upper-ocean thermal structure. Understanding the typhoon-induced oceanic response may help to improve the prediction of typhoon rainstorms and intensity. The present study compares the responses to Typhoon Megi (2010) of the SCS and NWP using an ocean model (POM), TMI satellite data, and ARGO float data. The results can be summarized as follows:

Both in the SCS and NWP, the typhoon-induced cold wake strongly depends on the typhoon's intensity and translation speed, and the upper-ocean states, which include the MLD and oceanic stratification. However, the upper-ocean response induced by the typhoon differs significantly between the SCS and NWP. First, the typhoon-induced SST and MLT cooling in the SCS are obviously stronger than those in the NWP, which can be primarily attributed to the different oceanic upwelling and entrainment mixing over these two regions. Second, the amplitude of near-inertial currents tends to decrease with depth. When the typhoon enters into the SCS, the most striking features of the response to Typhoon Megi (2010) are that the vertical structure of the near-inertial current exhibits a two-layer pattern, layered at the depth of 80 m, where the inertial currents in the upper layer are about 180° out-of-phase with those in the lower layer. However, such a vertical structure tends to disappear when the vertical thermal stratification weakens in the NWP. Finally, the vertical velocity tends to decrease with depth, with alternating upwelling and downwelling along the typhoon track, both in the SCS and the NWP.

Acknowledgements. The authors are grateful to the two anonymous reviewers for their helpful comments. This work was supported by the National Key Basic Research and Development Plan (Grant No. 2015CB953900), the National Natural Science Foundation of China (Grant No. 41176005), the Public Science and Technology Research Funds Projects of the Ocean (Grant No. GYHY201105018), and the China R&D Special Fund for Public Welfare Industry (GYHY 201306016).

REFERENCES

Antonov, J. A., R. A. Locarnini, T. P. Boyer, H. E. Garcia, and A. V. Mishonov, 2006: *Salinity.* Vol. 2, *World Ocean Atlas 2005*, NOAA Atlas NESDIS 62, Levitus, S, Ed., U.S. Government Printing Office, Washington, D.C., 182 pp.

Bender, M. A., and I. Ginis, 2000: Real-case simulations of hurricane-ocean interaction using a high-resolution coupled model: Effects on hurricane intensity. *Mon. Wea. Rev.*, **128**, 917–946, doi: 10.1175/1520-0493(2000)128<0917:RCSOHO>2.0.CO;2.

Chang, S. W., and R. A. Anthes, 1979: The mutual response of the tropical cyclone and the ocean. *J. Phys. Oceanogr.*, **9**, 128–135, doi: 10.1175/1520-0485(1979)009<0128:TMROTT>2.0.CO;2.

Chen, X. Y., D. L. Pan, X. Q. He, Y. Bai, and D. F. Wang, 2012: Upper ocean responses to category 5 typhoon Megi in the western north Pacific. *Acta Oceanologica Sinica*, **31**(1), 51–58.

Chiang, T.-L., C.-R. Wu, and L.-Y. Oey, 2011: Typhoon Kai-Tak: An ocean's perfect storm. *J. Phys. Oceanogr.*, **41**, 221–233.

Choi, Y., K.-S. Yun, K.-J. Ha, K.-Y. Kim, S.-J. Yoon, and J. C. L. Chan, 2013: Effects of asymmetric SST distribution on straight-moving typhoon Ewiniar (2006) and recurving typhoon Maemi (2003). *Mon. Wea. Rev.*, **141**, 3950–3967, doi: 10.1175/MWR-D-12-00207.1.

Chu, P. C., J. M. Veneziano, C. W. Fan, M. J. Carron, and W. T. Liu, 2000: Response of the south China sea to tropical cyclone Ernie 1996. *J. Geophys. Res.*, **105**(C6), 13 991–14 009.

Da Silva, A., A. C. Young, and S. Levitus, 1994: *Atlas of Surface Marine Data 1994*. NOAA Atlas NESDIS 9, U.S. Department of Commerce, NOAA, NESDIS, 308 pp.

Elsberry, R. L., T. Fraim, and R. N. Trapnell Jr, 1976: A mixed layer model of the oceanic thermal response to hurricanes. *J. Geophys. Res.*, **81**, 1153–1162.

Elsner, J. B., S. E. Strazzo, T. H. Jagger, T. LaRow, and M. Zhao, 2013: Sensitivity of limiting hurricane intensity to SST in the Atlantic from observations and GCMs. *J. Climate*, **26**, 5949–5957, doi: 10.1175/JCLI-D-12-00433.1

Fisher, E. L., 1958: Hurricanes and the sea-surface temperature field. *J. Meteor.*, **15**, 328–333.

Garrett, C., 2001: What is the "near-inertial" band and why is it different from the rest of the internal wave spectrum. *J. Phys. Oceanogr.*, **31**(4), 962–971.

Geisler, J. E., 1970: Linear theory of the response of a two layer ocean to a moving hurricane. *Geophys. Fluid Dyn.*, **1**, 249–272.

Gill, A. E., 1984: On the behavior of internal waves in the wakes of storms. *J. Phys. Oceanogr.*, **14**, 1129–1151.

Gjevik, B., 1991: Simulations of shelf sea response due to travelling storms. *Cont. Shelf Res.*, **11**(2), 136–166.

Gjevik, B., and M. A. Merrifield, 1993: Shelf-sea response to tropical storms along the west coast of Mexico. *Cont. Shelf Res.*, **13**(1), 25–47.

Greatbatch, R. J., 1985: On the role played by upwelling of water in lowering sea surface temperatures during the passage of a storm. *J. Geophys. Res.*, **20**, 11 751–11 755.

Guan, S. D., W. Zhao, J. Huthnance, J. W. Tian, and J. H. Wang, 2014: Observed upper ocean response to typhoon Megi (2010) in the Northern South China Sea, *J. Geophys. Res.*, **119**, 3134–3157, doi: 10.1002/2013JC009661.

Halpern, D., 1974: Observations of the deepening of the wind-mixed layer in the northeast Pacific Ocean. *J. Phys. Oceanogr.*, **4**, 454–466.

Kalnay, E, and Coauthors, 1996: The NCEP/NCAR 40-year reanalysis project. *Bull. Amer. Meteor. Soc.*, **77**, 437–470.

Ko, D. S., S.-Y. Chao, C.-C. Wu, and I.-I. Lin, 2014: Impacts of typhoon Megi (2010) on the South China Sea. *J. Geophys. Res.*, **119**, 4474–4489, doi: 10.1002/2013JC009785.

Large, W. G., and G. B. Crawford, 1995: Observations and simulations of upper-ocean response to wind events during the Ocean Storms Experiment, *J. Phys. Oceanogr.*, **25**, 2831–2852.

Leiper, D. F., 1967: Observed ocean conditions and hurricane Hilda, 1964. *J. Atmos. Sci*., **24**, 182–196.

Levitus, S., 1982: *Climatological Atlas of the World Ocean*. NOAA Professional Paper No. 13, 191 pp.

Lin, I.-I., 2012: Typhoon-induced phytoplankton blooms and primary productivity increase in the western North Pacific subtropical ocean. *J. Geophys. Res*., **117**, C03039, doi: 10.1029/2011JC007626.

Lin, I.-I., and Coauthors, 2003a: New evidence for enhanced ocean primary production triggered by tropical cyclone, *Geophys. Res. Lett*., **30**(13), 1718, doi: 10.1029/2003GL017141.

Lin, I.-I., W. T. Liu, C.-C. Wu, J. C. H. Chiang, and C.-H. Sui, 2003b: Satellite observations of modulation of surface winds by typhoon-induced upper ocean cooling. *Geophys. Res. Lett*., **30**, 1131, doi: 10.1029/2002GL015674.

Liu L., J. F. Fei, X. P. Cheng, and X. G. Huang, 2013: Effect of wind-current interaction on ocean response during Typhoon KAEMI (2006). *Science China Earth Sciences*, **56**(3), 418–433.

Locarnini, R. A., A. V. Mishonov, J. I. Antonov, T. P. Boyer, and H. E. Garcia, 2006: *Temperature*. Vol. 1, *World Ocean Atlas 2005*, NOAA Atlas NESDIS 61, L. Levitus, Ed., U.S. Government Printing Office, Washington, D.C., 182 pp.

Mei, W., and C. Pasquero, 2013: Spatial and temporal characterization of sea surface temperature response to tropical cyclones. *J. Climate*, **26**, 3745–3765, doi: 10.1175/JCLI-D-12-00125.1.

Mei, W., M. Lie, I.-I. Lin, and S.-P. Xie, 2015b: Tropical cyclone-induced ocean response: A comparative study of the South China Sea and tropical Northwest Pacific. *J. Climate*, **28**(15), 5952–5968, doi: 10.1175/JCLI-D-14-00651.1.

Mei, W., S.-P. Xie, M. Zhao, and Y. Q. Wang, 2015a: Forced and internal variability of tropical cyclone track density in the western North Pacific. *J. Climate*, **28**, 143–167, doi: 10.1175/JCLI-D-14-00164.1.

Miller, B. J., 1964: A study of the filling of Hurricane Donna (1960) over land. *Mon. Wea. Rev*., **92**, 389–406.

Millot, C., and M. Crépon, 1981: Inertial oscillations on the continental shelf of the gulf of lions-observations and theory. *J. Phys. Oceanogr*., **11**, 639–657, doi: 10.1175/1520-0485(1981)011<0639:IOOTCS>2.0.CO;2.

Morey, S. L., M. A. Bourassa, D. S. Dukhovskoy, and J. J. O'Brien, 2006: Modeling studies of the upper ocean response to a tropical cyclone. *Ocean Dynamics*, **56**, 594–606, doi: 10.1007/s10236-006-0085-y.

O'Brien, J. J., 1967: The non-linear response of a two-layer, baroclinic ocean to a stationary, axially-symmetric hurricane: Part II. Upwelling and mixing induced by momentum transfer. *J. Atmos. Sci*., **24**, 208–215.

O'Brien, J. J., and R. O. Reid, 1967: The non-linear response of a two-layer, baroclinic ocean to a stationary, axially-symmetric hurricane: Part I. Upwelling induced by momentum transfer. *J. Atmos. Sci*., **24**, 197–207.

Oey, L.-Y., M. Inoue, R. Lai, X.-H. Lin, S. E. Welsh, and L. J. Rouse Jr, 2008: Stalling of near-inertial waves in a cyclone, *Geophys. Res. Lett*., **35**, L12604, doi: 10.1029/2008GL034273.

Price, J. F., 1981: Upper ocean response to a hurricane. *J. Phys. Oceanogr*., **11**, 153–175.

Price, J. F., T. B. Sanford, and G. Z. Forristall, 1994: Forced stage response to a moving hurricane. *J. Phys. Oceanogr*., **24**, 233–260.

Sakaida, F., H. Kawamura, and Y. Toba, 1998: Sea surface cooling caused by typhoons in the Tohoku Area in August 1989. *J. Geophys. Res*., **103**(C1), 1053–1065.

Shang, S. L., and Coauthors, 2008: Changes of temperature and bio-optical properties in the South China Sea in response to typhoon Lingling, 2001. *Geophys. Res. Lett*., **35**, L10602, doi: 10.1029/2008GL033502.

Shay, L. K., and R. L. Elsberry, 1987: Near-inertial ocean current response to hurricane Frederic. *J. Phys. Oceanogr*., **17**, 1249–1269.

Shay, L. K., P. G. Black, A. J. Mariano, J. D. Hawkins, and R. L. Elsberry, 1992: Upper ocean response to Hurricane Gilbert. *J. Geophys. Res*., **97**, 20 227–20 248.

Slutz, R. J., S. J. Lubker, J. D. Hiscox, S. D. Woodruff, R. L. Jenne, D. H. Joseph, P. M. Steurer, and J. D. Elms, 1985: COADS (comprehensive ocean-atmosphere data set), Release 1. NOAA Environmental Research Laboratories, CIRES University of Colorado, 300 pp.

Stramma, L., P. Cornillon, and J. F. Price, 1986: Satellite observations of sea surface cooling by hurricanes. *J. Geophys. Res*., **91**(C4), 5031–5035.

Tsai, Y., C.-S. Chern, and J. Wang, 2012: Numerical study of typhoon-induced ocean thermal content variations on the northern shelf of the South China Sea. *Cont. Shelf Res*., **42**, 64–77.

Tseng, Y.-H., S. Jan, D. E. Dietrich, I.-I. Lin, Y.-T. Chang, and T.-Y. Tang, 2010: Modeled oceanic response and sea surface cooling to typhoon Kai-Tak. *Terrestrial, Atmospheric and Oceanic Sciences*, **21**, 85–98, doi: 10.3319/TAO.2009.06.08.02(IWNOP).

Wang, J. C., J. Zhang, and J. G. Yang, 2014: Numerical simulation and preliminary analysis on ocean waves during Typhoon Nesat in South China Sea and adjacent areas. *Chinese Journal of Oceanology and Limnology*, 2014, **32**(3), 665–680.

Yablonsky, R. M., and I. Ginis, 2009: Limitation of one-dimensional ocean models for coupled hurricane-ocean model forecasts. *Mon. Wea. Rev*., **137**, 4410–4419, doi: 10.1175/2009MWR2863.1

Yang, Y.-J., L. Sun, A.-M. Duan, Y.-B. Li, Y.-F. Fu, Y.-F. Yan, Z.-Q. Wang, and T. Xian, 2012: Impacts of the binary typhoons on upper ocean environments in November 2007. *Journal of Applied Remote Sensing*, **6**, 063583, doi: 10.1117/1.JRS.6.063583.

Yun, K.-S., J. C. L. Chan, and K.-J. Ha, 2012: Effects of SST magnitude and gradient on typhoon tracks around East Asia: a case study for Typhoon Maemi (2003). *Atmospheric Research*, **109-110**, 36–51.

Zedler, S. E., T. D. Dickey, S. C. Doney, J. F. Price, X. Yu, and G. L. Mellor, 2002: Analyses and simulations of the upper ocean's response to Hurricane Felix at the Bermuda Testbed Mooring site: 13-23 August 1995. *J. Geophys. Res*., **107**(C12), 25-1–25-29, doi: 10.1029/2001JC000969.